Journal of Applied Mechanics and Technical Physics, Vol. 39, No. 1, 1998

DEVELOPED TURBULENT FLOW IN A PLANE CHANNEL WITH SIMULTANEOUS INJECTION THROUGH ONE POROUS WALL AND SUCTION THROUGH THE OTHER

U. K. Zhapbasbaev and G. Z. Isakhanova

UDC 532.542

Results of a numerical-theoretical study of a developed turbulent flow of an incompressible fluid in a plane channel with simultaneous injection of mass through one porous wall and suction of the same mass through the other are presented. The system of equations of averaged motion is closed using a turbulent-stress model. The calculated data of the mean and fluctuational characteristics are in reasonable agreement with experimental results for two values of the Reynolds number of the main flow (Re = 10,400 *and* 34,000).

Introduction. Turbulent flows with mass transfer through porous walls have a number of special features (mass injection leads to flow turbulization, while mass suction causes flow laminarization) and are widely used in practice. The majority of experimental and numerical-theoretical studies are devoted to turbulent motion in a round pipe [1]. Considerable success has been achieved in understanding the laws of distribution of the mean and fluctuational characteristics of the flow. Calculation results obtained using advanced turbulence models are in reasonable agreement with experimental results [1, 2]. In contrast to turbulent flow in a round pipe, motion in a plane channel with simultaneous injection through one wall and suction through the other is characterized by asymmetry of the boundary actions. Calculations should, therefore, be performed from one wall to the other, rather than from the central plane of the channel. A certain analog of this kind of channel flow is turbulent motion in a plane channel one wall of which is rough and the other smooth [3]. A study showed that asymmetric boundary conditions affect appreciably the turbulent state of the flow [3, 4]. The calculation was performed using a Reynolds stress model, and reasonable agreement of numerical and experimental data was obtained [4]. Like the motion in a channel with one rough wall the flow in a plane channel with simultaneous injection of mass through one porous wall and its suction through the other can become fully turbulent, which is very important for evaluation of current semiempirical theories of turbulence. In this aspect, the examined turbulent flow can be used as a test case for description of channel flows with mass transfer through porous walls. The present paper is devoted to evaluation of a turbulence model by comparing numerical and experimental results.

1. Physicomathematical Flow Model. We consider a turbulent flow in a plane channel with porous walls. The channel width is $2B = 0.45$ m and its height is $2H = 0.034$ m, as under experimental conditions. Let the mass be injected through the lower wall and suction of the same mass occur through the upper wall; thus, the flow rate of the main stream does not change. Since the injection and suction velocities are equal and constant, the fluid motion is stabilized, and at a certain distance from the beginning of mass transfer the mean and fluctuational characteristics do not change in the stream direction. On the average, the flow considered is plane and fully turbulent; thus, all the flow parameters depend only on the transverse flow coordinate. The Ox_1 axis is directed along the lower channel wall, and the Ox_2 axis is directed along the channel height. In

Al-Farabi Kazakh National State University, Almaty 480121. Translated from Prikladnaya Mekhanika i Tekhnicheskaya Fizika, Vol. 39, No. 1, pp. 61–68, January–February, 1998. Original article submitted March 19, 1996; revision submitted May 7, 1996.

0021-8944/98/3901-0053 $20.00

accordance with these assumptions, we can write the following equation of motion in dimensionless variables:

$$V_w \frac{dU_1}{dx_2} = -\frac{dP}{dx_1} + \frac{1}{\mathrm{Re}} \frac{d^2U_1}{dx_2^2} - \frac{d\langle u_1 u_2 \rangle}{dx_2}. \tag{1.1}$$

Here the reference scale of velocity is the mass-mean velocity U_0, and the reference scale of length is half the channel height H ($\mathrm{Re} = U_0 H/\nu$ is the Reynolds number and $V_w = v_w/U_0$ is the mass-transfer velocity). The pressure gradient is found from the condition of conservation of mass flow

$$\int_0^2 U_1 dx_2 = 2. \tag{1.2}$$

System (1.1) and (1.2) is closed using a Reynolds stress model [2, 5], which has the following form for the problem considered and low Reynolds numbers:

$$V_w \frac{d\langle u_i u_j \rangle}{dx_2} = \frac{d}{dx_2}\left(\frac{1}{\mathrm{Re}} \frac{d\langle u_i u_j \rangle}{dx_2} - J_{ijk}\right) + P_{ij} + \Phi_{ij} - \varepsilon_{ij}, \tag{1.3}$$

where P_{ij} is the generation of Reynolds stress because of the mean shear, Φ_{ij} is the correlation of pressure fluctuations with the deformation rate, J_{ijk} is the turbulent diffusion flow, and ε_{ij} is the viscous dissipation.

The relation for ε_{ij} is represented in the form [6]

$$\varepsilon_{ij} = \frac{2}{3}\varepsilon\delta_{ij} + \frac{2}{\mathrm{Re}} \frac{\delta_{im}\delta_{jn}}{y^2} \langle u_m u_n \rangle, \tag{1.4}$$

where ε is the dissipation rate of the kinetic energy of turbulence and y is the normal coordinate reckoned each time from the wall.

In accordance with Eq. (1.4), the transport equation of the dissipation rate of the kinetic energy of turbulence ε is written in Chien's form [6]

$$V_w \frac{d\varepsilon}{dx_2} = \frac{d}{dx_2}\left[\left(\frac{1}{\mathrm{Re}} + C_\sigma \frac{k\langle u_2^2 \rangle}{\varepsilon}\right) \frac{d\varepsilon}{dx_2}\right] + C_{1\varepsilon} \frac{\varepsilon}{k} P_k - C_{2\varepsilon} f_\varepsilon \frac{\varepsilon^2}{k} - \frac{2g_\varepsilon \varepsilon}{\mathrm{Re}\, y^2}, \tag{1.5}$$

where P_k is the generation of the kinetic energy of turbulence k. The transport equation for the kinetic energy of turbulence can easily be derived from (1.3) by convolution with respect to the subscripts i and j:

$$V_w \frac{dk}{dx_2} = \frac{d}{dx_2}\left(\frac{1}{\mathrm{Re}} \frac{dk}{dx_2} - \frac{J_{iik}}{2}\right) - \varepsilon - \frac{2k}{\mathrm{Re}\, y^2}. \tag{1.6}$$

It is convenient to use this equation in calculations instead of the equation for $\langle u_3^2 \rangle$.

Two relations were used for approximation of Φ_{ij} in (1.3): the first relation, which was proposed in [7], is

$$\Phi_{ij} = -C_1 \frac{\varepsilon}{k}\left(\langle u_i u_j \rangle - \frac{2}{3}\delta_{ij}k\right)$$

$$-\frac{C_2 + 8}{11}\left(P_{ij} - \frac{2}{3}\delta_{ij}P_k\right) - \frac{8C_2 - 2}{11}\left(D_{ij} - \frac{2}{3}\delta_{ij}P_k\right) - \frac{30\,C_2 - 2}{55} k\left(\frac{\partial U_i}{\partial x_j} + \frac{\partial U_j}{\partial x_i}\right) + \Phi_{ijw}; \tag{1.7}$$

the second, more simplified one, which was proposed in [8], is

$$\Phi_{ij} = -C_1 \frac{\varepsilon}{k}\left(\langle u_i u_j \rangle - \frac{2}{3}\delta_{ij}k\right) - 0.6\left(P_{ij} - \frac{2}{3}\delta_{ij}P_k\right) + \Phi_{ijw}. \tag{1.8}$$

Here

$$D_{ij} = -\left(\langle u_i u_k \rangle \frac{\partial U_k}{\partial x_j} + \langle u_j u_k \rangle \frac{\partial U_k}{\partial x_i}\right); \quad \Phi_{ijw} = \left[C_3\left(P_{ij} - \frac{2}{3}\delta_{ij}P_k\right) + C_4 k\left(\frac{\partial U_i}{\partial x_j} + \frac{\partial U_j}{\partial x_i}\right)\right] f_w,$$

where Φ_{ijw} is a near-wall correction for Φ_{ij}.

TABLE 1

Model version	Approximation for Φ_{ij}			Approximation for J_{ijk}	
	relation		$\Phi_{ijw} = 0$	relation	
	(1.7)	(1.8)		(1.9)	(1.10)
A1	+			+	
A2	+		+	+	
A3	+		+		+
B1		+		+	
B2		+	+	+	
B3		+	+		+

Note. The plus sign means that the relation was used in the model version to approximate Φ_{ij} or J_{ijk}.

The diffusion flow J_{ijk} in (1.3) was found from the formula [4]

$$J_{ijk} = -C_s \frac{k}{\varepsilon}\left(\langle u_i u_n\rangle \frac{\partial\langle u_j u_k\rangle}{\partial x_n} + \langle u_j u_n\rangle \frac{\partial\langle u_k u_i\rangle}{\partial x_n} + \langle u_k u_n\rangle \frac{\partial\langle u_i u_j\rangle}{\partial x_n}\right). \tag{1.9}$$

A simpler analog of (1.9) was given in [9]:

$$J_{ijk} = -0.22 \frac{k}{\varepsilon}\langle u_2^2\rangle \frac{d\langle u_i u_j\rangle}{dx_2}. \tag{1.10}$$

In the calculations, use was made of various versions of the model (1.3) that differ from each other by the method of approximation of Φ_{ij} and J_{ijk} (see Table 1). System (1.3)–(1.9) includes the constants and near-wall functions $C_1 = 1.5$, $C_2 = 0.4$, $C_3 = 0.45$, $C_4 = 0.08$, $C_s = 0.11$, $C_{1e} = 1.35$, $C_{2e} = 1.8$, $C_\sigma = 0.15$, $g_e = \exp(-0.5 y V_* \mathrm{Re})$, $f_e = 1 - (1/2)\exp[-k^2\mathrm{Re}/(6\varepsilon)]$, and $V_* = v_*/U_0$ (v_* is the dynamic velocity without mass transfer). The near-wall function was found using Cebeci's hypothesis [9] and it is represented by the dependence $f_w = \exp(-2y\mathrm{Re}\, V_*/A)$, where

$$A = 26\left\{-\frac{P_*}{V_{w*}}\exp(11.8V_{w*} - 1) + \exp(11.8V_{w*})\right\}^{1/2}; \quad P_* = -\frac{dP}{dx_1}\frac{1}{\mathrm{Re}\, V_*^3}; \quad V_{w*} = \frac{V_w}{V_*}.$$

System of equations of motion (1.1) and (1.2) is solved together with the transport equations $\langle u_1^2\rangle$, $\langle u_2^2\rangle$, k, $\langle u_1 u_2\rangle$, and ε under the boundary conditions

$$x_2 = 0: \quad U_1 = 0, \langle u_1^2\rangle = \langle u_2^2\rangle = \langle u_1 u_2\rangle = k = \varepsilon = 0,$$

$$x_2 = 2: \quad U_1 = 0, \langle u_1^2\rangle = \langle u_2^2\rangle = \langle u_1 u_2\rangle = k = \varepsilon = 0.$$

A grid with a variable step is used for numerical integration of the system. As a rule, 5 nodes are concentrated near the wall ($0 \leqslant x_{2*} \leqslant 5$ and $x_{2*} = x_2 V_* \mathrm{Re}$), the next 12 nodes lie at a distance of $5 \leqslant x_{2*} \leqslant 65$ from the wall, and the most distant region from the wall ($65 \leqslant x_{2*} \leqslant V_*\mathrm{Re}$) has 30 to 50 nodes, depending on the Reynolds number. A numerical solution of the system of ordinary differential equations is obtained by Newton's iteration technique. The pressure gradient was determined by the splitting method [10] from the condition of mass flow conservation (1.2). The model and the numerical method were checked by comparison of numerical data and experimental results obtained in a study [11] of a developed turbulent flow in a plane channel without mass transfer through the walls. Calculated test data for the longitudinal velocity component U_1 and the root-mean-square longitudinal component of velocity fluctuations $\sqrt{\langle u_1^2\rangle}$ are in satisfactory agreement with experimental data (Fig. 1, where calculated data and experimental data [11] are shown by curves and points, respectively).

2. Discussion of the Calculated Results. The main regime parameters of the flow are Re and V_w. The numerical experiment was performed in the range of regime parameters $4 \cdot 10^3 \leqslant \mathrm{Re} \leqslant 4 \cdot 10^4$

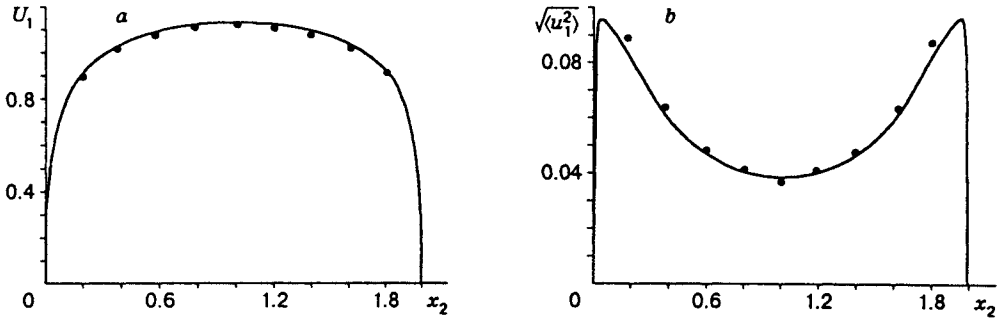

Fig. 1

and $0 \leqslant V_w \leqslant 0.01$. Detailed numerical data were obtained for Re = 10,400 and 34,000 in accordance with experimental conditions [12]. Both in experiments and in calculations, the mass transfer velocity was $V_w = 0$, 0.002, 0.004, 0.006, and 0.009 for Re = 10,400 and $V_w = 0$, 0.001, 0.0018, 0.0025, and 0.0033 for Re = 34,000. Available experimental profiles of the longitudinal velocity component U_1, the root-mean-square components of the longitudinal $\sqrt{\langle u_1^2 \rangle}$ and transverse $\sqrt{\langle u_2^2 \rangle}$ velocity fluctuations, and the turbulent friction $\langle u_1 u_2 \rangle$ allowed one to evaluate the applicability of one or another version of the Reynolds stress model (1.3).

A comparative analysis of the calculated distributions showed satisfactory agreement with the experimental distributions of U_1, $\sqrt{\langle u_1^2 \rangle}$, and $\langle u_1 u_2 \rangle$ for version A2 (see Table 1), although the calculated distributions of $\sqrt{\langle u_2^2 \rangle}$ are still different from the experimental ones. The near-wall correction Φ_{ijw} has only a slight effect on the calculated curves. The simplified relation for J_{ijk} from (1.10) increases somewhat the values of $\sqrt{\langle u_1^2 \rangle}$ and $\sqrt{\langle u_2^2 \rangle}$ in the turbulent core flow in comparison with the experimental data for $\sqrt{\langle u_1^2 \rangle}$ and $\sqrt{\langle u_2^2 \rangle}$. The calculations performed with account for Eq. (1.8) for Φ_{ij} are in poor agreement with experiment. Based on a preliminary analysis, we chose version A2 for numerical-theoretical studies.

Figure 2 shows distributions of the longitudinal velocity component U_1 for various values of the mass-transfer velocity V_w and Re = 10,400 (here and in subsequent figures, calculated and experimental data [12] are shown by curves and points, respectively). It is seen that, for $V_w = 0$, the U_1 profile is symmetric about the central plane of the channel, with a maximum velocity value ($U_{1\,\max} = 1.16$). The calculated distribution of U_1 in the laminar sublayer, transitional region, and turbulent core flow yields an adequate description of the turbulent flow in the plane channel. Mass transfer is responsible for deformation of the U_1 profile. The distribution of U_1 becomes asymmetric about the central plane, levels out near the wall where injection occurs, and, conversely, fills out near the wall where suction occurs. The maximum of the velocity U_1 is shifted from the symmetry plane toward the upper boundary and is located where the turbulent friction $\langle u_1 u_2 \rangle$ is compensated by the shear stress of the channel walls and the transverse convection of momentum. The larger the value of V_w, the more noticeable the deformation of the U_1 profile. For the largest value of the mass-transfer velocity ($V_w = 0.009$) reached in the experiment, the maximum of U_1 is in the immediate vicinity of the wall where mass suction occurs.

This circumstance can be explained only by the fact that the turbulent friction $\langle u_1 u_2 \rangle$ near this wall decreases strongly as a result of suction of the boundary layer (Fig. 3, where profiles of $\langle u_1 u_2 \rangle$ are constructed for regime parameters corresponding to the U_1 distribution). It is easily seen that the larger the value of V_w, the larger the increase in $\langle u_1 u_2 \rangle$ on the side of injection. Being symmetric about the channel centerline, the initially linear distribution of $\langle u_1 u_2 \rangle$ for $V_w = 0$ becomes asymmetric with increasing V_w. A strong increase in $\langle u_1 u_2 \rangle$ is observed at the surface where the mass is injected.

The largest value of $\langle u_1 u_2 \rangle$, which, as a rule, is equal to the shear stress on the wall with $V_w = 0$. begins to move into the stream. As V_w increases, a larger part of the channel cross section is affected by the transverse convection of momentum, and the shear stress of the wall affects only the surface where the mass is sucked out. The zero value of $\langle u_1 u_2 \rangle$ is shifted from the central plane of the channel, and its location x_{20} does not coincide with the coordinate x_{2m} of the maximum value of the longitudinal velocity component U_{1m}. The

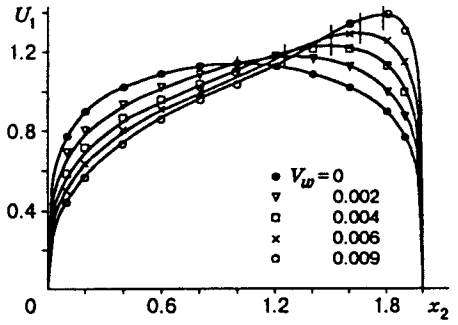

Fig. 2

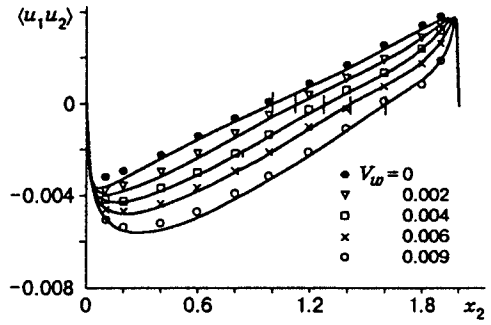

Fig. 3

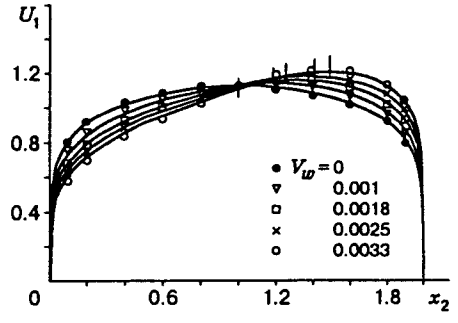

Fig. 4

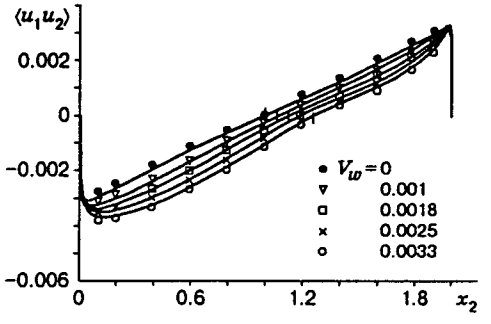

Fig. 5

coordinate x_{2m} lies closer to the channel wall. The calculated data show that the values of U_1, as a whole, correlate with the $\langle u_1 u_2 \rangle$ distribution and are in reasonable agreement with experimental results for all values of the mass-transfer velocity V_w.

Results for U_1 and $\langle u_1 u_2 \rangle$ calculated for Re = 34,000 are plotted in Figs. 4 and 5. Qualitatively, the profiles of U_1 and $\langle u_1 u_2 \rangle$ possess the aforementioned features. However, there are some quantitative differences: (1) the turbulent core flow occupies a large part of the channel cross section; (2) because of the smaller value of V_w, the deformation of the profiles of U_1 and $\langle u_1 u_2 \rangle$ is less noticeable than for Re = 10,400; (3) the experimental data are in reasonable agreement with the calculated data (curves of U_1 and $\langle u_1 u_2 \rangle$).

Figure 6 shows profiles of the root-mean-square components of the longitudinal $\sqrt{\langle u_1^2 \rangle}$ (a) and transverse $\sqrt{\langle u_2^2 \rangle}$ (b) velocity fluctuations for Re = 10,400. A significant increase in the turbulence characteristics at the wall where mass injection occurs and their decrease at the surface where suction of the boundary layer occurs are observed. An increase in $\sqrt{\langle u_1^2 \rangle}$ and $\sqrt{\langle u_2^2 \rangle}$ near the lower boundary is observed, despite the fact that the gradient of the longitudinal velocity component U_1 decreases, and, thus, the turbulence generation owing to the mean motion becomes weaker. Here, the larger the value of V_w, the stronger the increase in $\sqrt{\langle u_1^2 \rangle}$ and $\sqrt{\langle u_2^2 \rangle}$. The maximum values of $\sqrt{\langle u_2^2 \rangle}$ and $\sqrt{\langle u_1^2 \rangle}$ are increased and are shifted into the depth of the turbulent core flow, and the minimum values leave the central plane of the channel toward the upper boundary. The values of $\sqrt{\langle u_1^2 \rangle}$ and $\sqrt{\langle u_2^2 \rangle}$ are decreased near the surface with mass suction, although the gradients of the longitudinal velocity component U_1 are significant in this region, and the turbulence generated by the averaged motion should be noticeable. The calculated data prove the fact that mass injection increases the values of the turbulence characteristics, and suction of the boundary layer decreases them. The results calculated for $\sqrt{\langle u_1^2 \rangle}$ are in reasonable agreement with the experimental data for all values of the mass-transfer velocity V_w, whereas the calculated values of $\sqrt{\langle u_2^2 \rangle}$ are significantly different from the experimental ones, although the qualitative behavior of $\sqrt{\langle u_2^2 \rangle}$ is similar to the distribution of $\sqrt{\langle u_1^2 \rangle}$ versus V_w.

Beginning from Re = 34,000, an increase in V_w does not lead to significant reconstruction of the

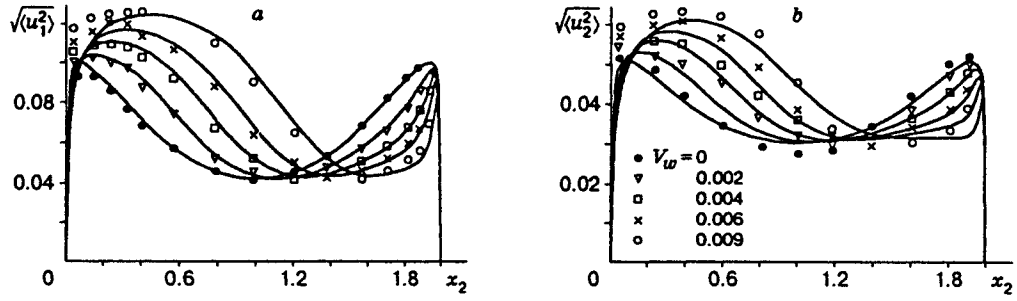

Fig. 6

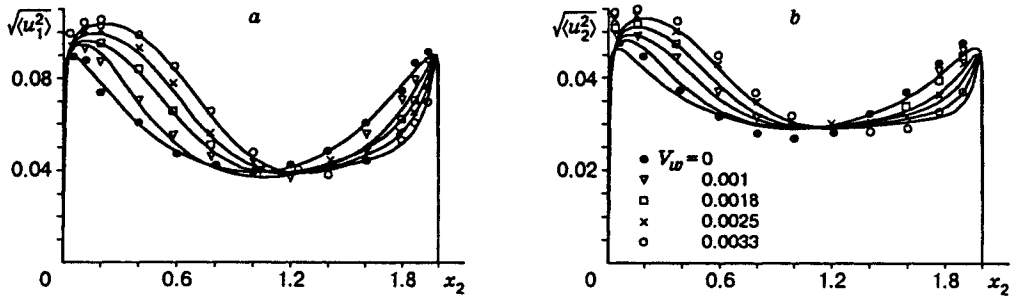

Fig. 7

profiles $\sqrt{\langle u_1^2 \rangle}$ and $\sqrt{\langle u_2^2 \rangle}$ (Fig. 7). The deformation of the profiles and their characteristic values (the maxima of $\sqrt{\langle u_1^2 \rangle}$ and $\sqrt{\langle u_2^2 \rangle}$ and the shift of the coordinate of the minima) are appreciably lower than for Re = 10,400. This can be explained not only by the smaller values of V_w but also by the growth of the flow turbulence at Re = 34,000. The calculated and experimental data for $\sqrt{\langle u_1^2 \rangle}$ are in reasonable agreement.

On the basis of the numerical-theoretical research, we can conclude that:

(1) supplemented by the equation of the dissipation rate of the kinetic energy of turbulence, the Reynolds stress model in version A2 can be used to describe a fully developed turbulent flow in a plane channel with simultaneous injection of mass through one porous wall and suction of the same mass through the other;

(2) the calculated data for the mean and fluctuational motion are in satisfactory agreement with the experimental data;

(3) fully developed flow in a plane channel with mass transfer through porous walls is a classical example where turbulization and laminarization effects occur simultaneously, and it can become a test case for evaluation of the capabilities of present-day turbulence models.

REFERENCES

1. V. M. Eroshenko and L. I. Zaichik, *Hydrodynamics and Heat and Mass Transfer on Permeable Surfaces* [in Russian], Nauka, Moscow (1984).
2. R. M. C. So and G. J. Yoo, "Low Reynolds number modeling of turbulent flows, with and without wall transpiration," *AIAA J.*, No. 12, 1556-1565 (1987).
3. K. Hanjalic and B. E. Launder, "Fully developed asymmetric flow in a plane channel," *J. Fluid Mech.*, **51**, Part 1, 301–324 (1972).
4. K. Hanjalic and B. E. Launder, "Reynolds-stress model of turbulence and its application to thin shear flows," *J. Fluid Mech.*, **52**, Part 4, 609–638 (1972).
5. Sh. A. Ershin, U. K. Zhapbasbaev, T. B. Kozhakhmetov, and A. V. Smol'yaninov, "Turbulent incompressible flow in a channel with one-sided mass transfer," *Prikl. Mekh. Tekh. Fiz.*, No. 1, 62–68 (1991).

6. K. Y. Chien, "Predictions of channel and boundary layer flows with low Reynolds-number two-equation model of turbulence," *AIAA J.*, **20**, No. 1, 33–38 (1982).
7. B. E. Launder, G. J. Reece, and W. Rodi, "Progress in the development of a Reynolds-stress turbulence closure," *J. Fluid Mech.*, **68**, Part 3, 537–566 (1975).
8. B. J. Daly and F. H. Harlow, "Transport equations of turbulence," *Phys. Fluids*, **13**, 2634–2649 (1970).
9. T. Cebeci, "Behavior of turbulent flow near a porous wall with pressure gradient," *AIAA J.*, **12**, No. 8, 24–29 (1970).
10. L. M. Simuni, "Motion of a viscous incompressible fluid in a plane pipe," *Zh. Vychisl. Mat. Mat. Fiz.*, **5**, No. 6, 1138–1141 (1965).
11. A. K. M. F. Hussain and W. C. Reynolds, "Measurements in fully developed turbulent channel flow," *Teor. Osnovy Inzh. Raschetov* (Transl. J. *Trans. ASME. J., Ser. E*), No. 4, 295–309 (1975).
12. U. K. Zhapbasbaev, T. B. Kozhakhmetov, A. V. Smol'yaninov, and N. Izimov, "Turbulent incompressible flow in a plane channel with injection and suction through porous walls," in: *Hydrodynamics and Heat and Mass Transfer in Complex Flows* [in Russian], Kazakh. Gos. Univ., Alma-Ata (1989), pp. 52–56.